Biophysical Journal
Article

Biophysical Society

Ions Modulate Key Interactions between pHLIP and Lipid Membranes

Justin Westerfield,[1] Chitrak Gupta,[2] Haden L. Scott,[1] Yujie Ye,[1] Alayna Cameron,[1] Blake Mertz,[2,3,*] and Francisco N. Barrera[1,*]

[1]Department of Biochemistry & Cellular and Molecular Biology, University of Tennessee-Knoxville, Knoxville, Tennessee; [2]C. Eugene Bennett Department of Chemistry and [3]WVU Cancer Institute, West Virginia University, Morgantown, West Virginia

ABSTRACT The pH-low insertion peptide (pHLIP) is used for targeted delivery of drug cargoes to acidic tissues such as tumors. The extracellular acidosis found in solid tumors triggers pHLIP to transition from a membrane-adsorbed state to fold into a transmembrane α-helix. Different factors influence the acidity required for pHLIP to insert into lipid membranes. One of them is the lipid headgroup composition, which defines the electrostatic profile of the membrane. However, the molecular interactions that drive the adsorption of pHLIP to the bilayer surface are poorly understood. In this study, we combine biophysical experiments and all-atom molecular dynamics simulations to understand the role played by electrostatics in the interaction between pHLIP and a 1-palmitoyl-2-oleoyl-*sn*-glycero-3-phosphocholine bilayer. We observed that the solution ionic strength affects the structure of pHLIP at the membrane surface as well as the acidity needed for different steps in the membrane insertion process. In particular, our simulations revealed that an increase in ionic strength affected both pHLIP and the bilayer; the coordination of sodium ions with the C-terminus of pHLIP led to localized changes in helicity, whereas the coordination of sodium ions with the phosphate moiety of the phosphocholine headgroups had a condensing effect on our model bilayer. These results are relevant to our understanding of environmental influences on the ability of pHLIP to adsorb to the cell membrane and are useful in our fundamental understanding of the absorption of pH-responsive peptides and cell-penetrating peptides.

SIGNIFICANCE The pH-low insertion peptide (pHLIP) is a membrane-active peptide with potential biomedical applications in targeted drug delivery and diagnostic imaging of disorders associated with acidosis (e.g., cancer). The general mechanism of binding, folding, and insertion of pHLIP are fairly well understood, but the molecular details of this process hold the key to the intelligent design of variants of pHLIP with enhanced properties. A pressing area of fundamental understanding is the effect of salt on pHLIP function. Our study uses a combination of experiment and simulation to unambiguously show how physiological salt concentrations cause localized changes in pHLIP function, in particular, decreasing the p*K* of insertion. Our results underscore the critical need to account for ionic strength in biophysical studies of pHLIP.

INTRODUCTION

The pH-low insertion peptide (pHLIP) is a water-soluble molecule that interacts with lipid membranes in a pH-dependent fashion. pHLIP can be found in three states based on its environment (1,2). In state I, in aqueous solution at neutral and basic pH, pHLIP adopts a random coil conformation. In state II, pHLIP adsorbs to the surface of lipid membranes in a similar conformation, with all its acidic residues remaining negatively charged (3). Upon a decrease in pH, the acidic residues in pHLIP are sequentially protonated, resulting in an increase in hydrophobicity. This causes the folding and insertion of pHLIP as a transmembrane helix (state III) (4). This mechanism is the driving force for the accumulation of pHLIP into solid tumors, which typically exhibit extracellular acidosis, and for delivery of drug cargoes into cancer cells (5).

The majority of biophysical studies on pHLIP have focused on modifications to the peptide and the resulting changes to function based on interactions with vesicles of the model lipid 1-palmitoyl-2-oleoyl-*sn*-3-phosphocholine (POPC) (4,6–15). However, the role of environmental factors

Submitted March 20, 2019, and accepted for publication July 22, 2019.

*Correspondence: blake.mertz@mail.wvu.edu or fbarrera@utk.edu

Justin Westerfield, Chitrak Gupta, and Haden L. Scott contributed equally to this work.

Editor: Sarah Veatch.

https://doi.org/10.1016/j.bpj.2019.07.034

and their effect on the function of pHLIP have recently garnered attention. The lipid composition of the membrane significantly affects the pH dependency of the insertion of pHLIP (16). For example, altering the membrane surface properties by incorporation of non-phosphocholine (PC) headgroups affects state II. Bilayers containing phosphatidylserine, phosphatidylethanolamine, and phosphatidylglycerol lead to shallower partitioning of pHLIP. Furthermore, in these conditions, states I and II are virtually indistinguishable by fluorescence spectroscopy (17–19). However, the molecular basis for the variable behavior of pHLIP in state II is poorly understood. This has direct implications to the function of pHLIP as changes in membrane composition and dynamics are a hallmark of many cellular phenomena. In particular, membrane asymmetry is disrupted in cancerous cells, leading to more phosphatidylserine exposure on the outer leaflet of the plasma membrane (20) and potentially altering the efficiency and specificity of pHLIP to target tumors. Intriguingly, the changes in state II observed with variations in lipid headgroup composition are often accompanied by large changes in the pK of insertion. We hypothesize that the shifts in pK of insertion result from changes in the membrane surface environment that directly affect the acidic groups of pHLIP in state II.

Although advances have been made in understanding the basis for these differences, we lack a comprehensive conceptual framework that describes the relationship between lipid composition and the binding, folding, and insertion of pHLIP. Characterizing these differences is intrinsically challenging because even slight modifications to the composition of the lipid bilayer affect multiple physical parameters of the membrane. However, understanding this biophysical relationship presents the opportunity to identify simpler ways to alter the properties of pHLIP. A key environmental aspect that has been largely overlooked is the role of salt in modulating the effect of electrostatics on the function of pHLIP. Here, we used a combination of experimental spectroscopic measurements and all-atom molecular dynamics (MD) simulations to characterize the ability of ionic conditions to alter state II and the pK of pHLIP. We observed that small changes in the buffer concentration changed the distribution of conformations of pHLIP in state II as well as the pH-dependent insertion into the membrane. These results highlight the delicate balance between environmental factors and the function of pHLIP that are critical in long-term development of applications using pH-dependent membrane-active peptides.

MATERIALS AND METHODS

Intrinsic tryptophan fluorescence

pHLIP (sequence: N_t-AAEQNPIYWARYADWLFTTPLLLLDLALLVDA DEGTCG-C_t) was synthesized using standard solid phase protocols (P3 BioSystems, Louisville, KY) and purified by reverse-phase high performance liquid chromatography to greater than 95% purity. It has been established that under our experimental conditions, pHLIP does not form a disulfide bond (8). Lyophilized peptide was dissolved in 10 mM sodium phosphate (NaP_i) buffer at pH 8.0, and concentration was determined via absorbance (ε_{280} = 13,940 M^{-1} cm^{-1}). POPC vesicles were prepared via extrusion through a 100-nm pore size membrane using a Mini Extruder (Avanti Polar Lipids, Alabaster, AL) in the same buffer to form large unilamellar vesicles via 31 passes. Next, pHLIP and POPC were incubated at room temperature for 1 h for a final lipid/peptide molar ratio of 200:1. Final peptide concentration was 1 μM. To perform a pH titration, the pH of different samples was adjusted by mixing with 100 mM stocks of sodium acetate, 2-(N-morpholino) ethanesulfonic acid, or HEPES ((4-(2-hydroxyethyl)-1-piperazineethanesulfonic acid)) buffers. The final pH of each sample was measured using a 2.5 mm-bulb pH electrode (Microelectrodes, Bedford, NH). Final buffer concentration of Na^+ was 19.3 mM (referred to as 19 mM for simplicity). Samples were also prepared at physiological ionic strength by the addition of 130.7 mM NaCl. Emission spectra were recorded using a Photon Technology International (Edison, NJ) QuantaMaster fluorometer at room temperature with the excitation wavelength set to 280 nm, the emission wavelength ranging from 310 to 400 nm, and excitation and emission slits set to 3 nm. Appropriate lipid blanks were subtracted in all cases. The data were analyzed by following the fluorescent emission intensity change at 335 nm, which is directly proportional to the population of molecular species present (21). Fluorescence intensity (FI) pH titrations were fitted to determine the pK using the following:

$$FI = \frac{F_a + F_b 10^{m(pH-pK)}}{1 + 10^{m(pH-pK)}}, \quad (1)$$

where F_a is the acidic baseline, F_b is the basic baseline, m is the slope of the transition, and pK is the midpoint of the curve (22).

Nitrobenzoxadiazole fluorescence assay

Conjugation of the environmentally sensitive dye nitrobenzoxadiazole (NBD) to the C-terminal cysteine in pHLIP was performed using IANBD (N, N′-dimethyl-N-(iodoacetyl)-N′-(7-nitrobenz-2-oxa-1,3-diazol-4-yl)ethylenediamine) (Thermo Fisher Scientific, Waltham, MA). The conjugated peptide (pHLIP-NBD) was purified by size exclusion chromatography using a PD-10 column (GE Healthcare Bio-Sciences, Marlborough, MA) in 1 mM NaP_i buffer (pH 7.5). The conjugation was verified by matrix-assisted laser desorption/ionization time of flight and high performance liquid chromatography, and samples were then aliquoted and lyophilized. Samples were rehydrated in 10 mM NaP_i (pH 8.0) at a final concentration of 0.8 μM (the NBD extinction coefficient used was 18,482 M^{-1} cm^{-1}) and incubated with POPC vesicles (prepared as described earlier) for 1 h. The pH of each row of a 96-well plate was adjusted using a series of 100 mM buffers (adding 14.3 μL of sodium acetate or NaP_i buffers). Fluorescence spectra were recorded at 25°C with excitation at 470 nm and an emission range of 520–600 nm using a Cytation 5 imaging plate reader (BioTek Instruments, Winooski, VT). The final pH was measured for each individual well of the plate. In the pH titrations, we monitored the emission FI at 540 nm. Data were fitted to Eq. 1 to determine the $pK_{Ct\text{-}NBD}$.

Circular dichroism

Lyophilized pHLIP was prepared as described previously. POPC vesicles were also prepared as described previously, except by the use of 3.2 mM NaP_i. Keeping NaP_i concentrations constant, salt concentration was changed using varying amounts of a 1 M NaCl stock. After 1 h incubation (with salt present), pH was adjusted with either 100 mM NaP_i (pH 8.02) (for a final pH of ~7.8) or 100 mM sodium acetate (pH 3.62) (for a final pH of ~3.8). CD measurements were performed using a 2-mm pathlength cuvette on a Jasco J-815 spectropolarimeter. All spectra were collected in the

presence of POPC vesicles at a lipid/peptide molar ratio of 150:1. Appropriate blanks were subtracted in all cases. High signal/noise ratios were present at all wavelengths as the voltage supplied to the photomultiplier tube never exceeded 700 V, per manufacturer recommendations. We averaged $\geq$30 scans with a scan rate of 100 nm/min and a bandwidth of 4 nm and a digital integration time of 4 s. Raw millidegree data were converted to mean residue ellipticity using the following:

$$[\theta]_{MRE} = \frac{\theta}{l \times (N-1) \times c^{*}1000}, \quad (2)$$

where θ is ellipticity in millidegrees, l is the pathlength in mm, N is the number of residues, and c is the concentration in M. Determination of the spectral minima was performed by applying a polynomial fit to the data from 195 to 210 nm. The polynomial fit was chosen over a Gaussian curve-fitting approach because of the asymmetry of the ~200 nm negative peak as a Gaussian fit skewed the minimal ellipticity toward higher wavelengths.

MD simulations

Coordinates for the pHLIP-POPC system were obtained by combining 1) snapshots from MD simulations of pHLIP in implicit solvent (23) and 2) generating a solvated POPC bilayer in http://www.charmm-gui.org (24–27) that was equilibrated for 47 ns in NAMD 2.12 (28) in the NPT ensemble at 310 K. Temperature was kept constant using Langevin dynamics with a damping coefficient of 1 ps^{-1}. Pressure was kept constant using Nose-Hoover Langevin piston with piston period of 50 fs. An anisotropic flexible cell was used to maintain a constant ratio of the unit cell in the x-y plane (80 Å). The cell dimension in the z axis was 130 Å (approximately a 90 Å water layer) to prevent pHLIP from interacting with the lower lipid leaflet in the neighboring periodic image. pHLIP was placed ~20 Å away from the bilayer surface (as measured by the distance between the centers of mass (COM) of pHLIP and the headgroups of the upper leaflet), overlapping waters were removed, and the system was further equilibrated for 3 ns. All systems had a lipid/peptide molar ratio of 200:1. Na^+ and Cl^- ions were added (in addition to the 5 Na^+ ions to neutralize pHLIP) to obtain a final salt concentration of 0, 20, 50, 100, and 150 mM (note that 0 mM corresponds to 5 Na^+ ions). These structures were then converted to Amber force field topologies (ff14SB (29), lipid14 (30), and the "optimal" 3-charge, 4-point rigid water model (31)) and further equilibrated in Amber16 (32) for 5 ns. This structure was used to seed five different simulations at each concentration in which the first 10 ns were discarded. Each production simulation was 400 ns long. In aggregate, a total of 10 μs of simulation was carried out.

Analysis of MD simulations

We used VMD (33) and home built tcl and Python scripts for data analysis. Matplotlib, gnuplot, and VMD were used for figure preparation. Helix-forming propensity was calculated in VMD and is defined using the STRIDE software (34), which identifies residues in pHLIP that undergo folding and satisfy the phi/psi requirements for classification as an α-helix.

RESULTS

The pK of insertion of pHLIP decreases with increasing salt concentration

The transition from state II to state III can be tracked by monitoring the changes in tryptophan fluorescence that result from the burial of pHLIP in the membrane. Insertion of pHLIP into the membrane is characterized by the staggered protonation of its different acidic groups: four aspartates, two glutamates, and the C_t group (3,4). We have recently reported that various ensemble fluorescence measurements result in distinct pK values (22), which can be ascribed to discrete steps in the coupled folding/membrane insertion process (6). Specifically, the pH midpoint determined by changes in tryptophan fluorescence, pK_{FI}, reports primarily on the local burial of the N_t half of pHLIP as it forms a helix on the membrane surface. As shown in Fig. 1 *A*, a pH drop caused a sigmoidal change in FI. When the experiment was repeated supplementing the buffer with close to physiological levels of NaCl (~131 mM), the pH-dependent transition shifted to more acidic pH values. In the absence of salt, pK_{FI} was 5.77 $\pm$ 0.10, whereas in the presence of NaCl, it was significantly lower at 5.37 $\pm$ 0.03 (Fig. 1 *B*). These results suggest that the presence of NaCl disfavors the protonation events that facilitate the membrane insertion of pHLIP.

We then determined the behavior of the C-terminal portion of pHLIP with both experiments and simulation. First, we conjugated the environmentally sensitive NBD dye to the cysteine residue present at the C_t of pHLIP, allowing us to determine $pK_{Ct\text{-}NBD}$. $pK_{Ct\text{-}NBD}$ reports on the final stages of membrane insertion of pHLIP, specifically the translocation of the C_t across the membrane that occurs at more acidic pH values (22). The FI and C_t-NBD of pHLIP are expected to have different transition midpoints because of the directionality of the insertion process. The highly negatively charged C_t requires more protonation events to facilitate traversing the hydrophobic core of the membrane. Therefore, the pK_{FI} is ~0.5 pH units higher than the $pK_{Ct\text{-}NBD}$ (22). The $pK_{Ct\text{-}NBD}$ also decreased from 5.2 to 4.6 in the presence of NaCl (Fig. 1 *B*, circles). When we performed atomistic MD simulations on systems with a similar series of salt concentrations, we observed that as the concentration of ions increased, the number of Na^+ ions clustered around the C-terminal acidic residues in pHLIP increases as well. (By taking the inverse of the number of Na^+ ions with the MD data, we mirror the same decreasing trend as with the pK of the experimental data.) Taken together, these results suggest that the presence of NaCl induces a change in pHLIP that requires increased acidity for membrane insertion to occur.

Increasing salt concentration leads to local effects on secondary structure in pHLIP

To determine the impact of the presence of NaCl on the secondary structure of pHLIP, we carried out circular dichroism (CD) spectroscopy. CD experiments performed in the presence of POPC vesicles at a neutral pH (state II) showed that both in the absence and presence of NaCl, pHLIP is largely unstructured as characterized by a weak signal at 222 nm, a characteristic minimum of α-helical structure (Fig. 2 *A*). However, a slight difference in the magnitude of the 222 nm signal was observed, larger than the SD of the

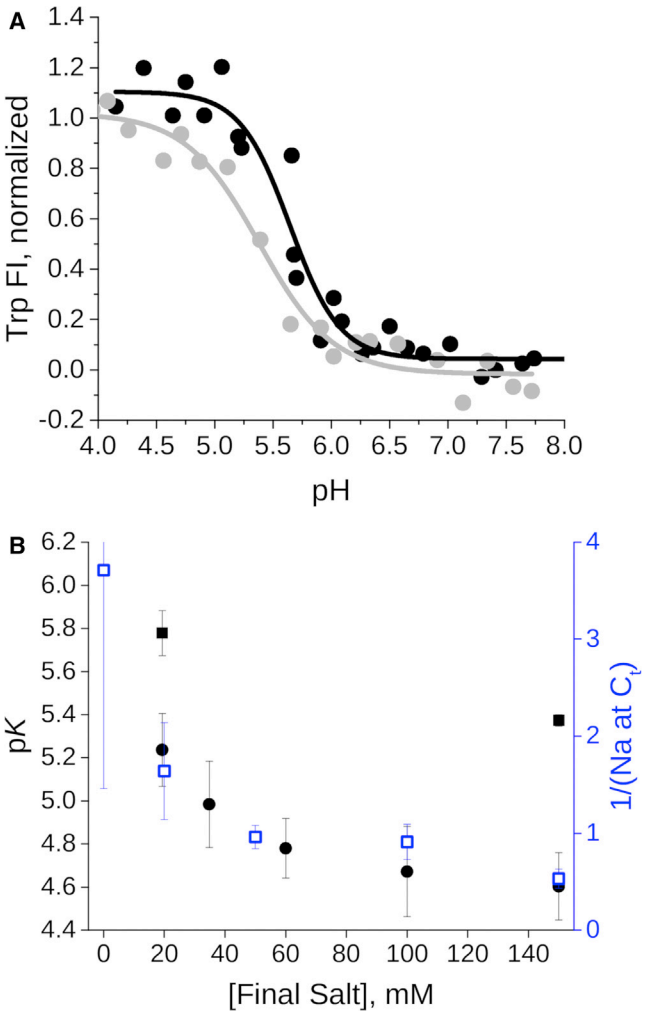

FIGURE 1 Ionic strength reduces the pK of pHLIP. (*A*) Shown are the representative pH titration curves, in which the normalized changes in Trp FI were fitted to Eq. 1 to yield pK_{FI}. Experiments were carried out varying the pH with different buffers (19 mM) and in the absence (*black symbols*) or the presence of 131 mM NaCl for a total [Na^+] of 150 mM (*gray symbols*). (*B*) The pK values obtained in (*A*) (*closed squares*, pKFI) are compared with those obtained following the intensity changes of NBD conjugated to the C_t of pHLIP (*circles*, p$K_{Ct\text{-}NBD}$). Means and SD are shown. $n = 3$–6. In addition, the number of Na^+ ions bound to the C_t acidic residues of pHLIP were quantified using MD simulations. Open squares show the inverse of the average number of Na^+ ions bound at the C_t. To see this figure in color, go online.

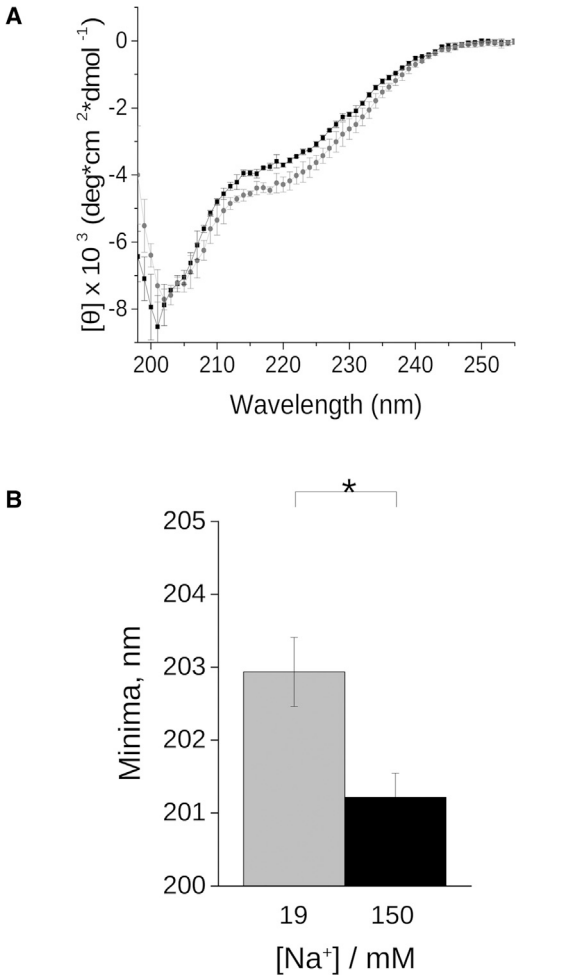

FIGURE 2 Ionic strength induces small but statistically significant helical changes in state II. (*A*) CD spectra are shown for pHLIP in the presence of 19 mM Na^+ (*gray*) or 150 mM Na^+ (*black*). Each data point corresponds to the mean ± SD. $n = 3$. (*B*) Spectral minimal determination is shown. Mean and SD are shown. $n = 7$. Statistical analysis was performed with a two-tailed Student's t-test; $*p < 0.05$. Experiments were performed in the presence of POPC at pH 7.9.

measurements. To further evaluate potential helical differences, we focused our attention on the lower wavelength region of the CD spectrum. A completely random coil polypeptide yields a CD spectrum with a single minimum at 200 nm (35). When a coiled polypeptide begins folding into an α-helix, this minimum undergoes a red shift, eventually ending at 208 nm upon the complete formation of an α-helix. When NaCl was added to pHLIP in state II, we observed a small blueshift of the minimum in the form of a statistically significant change from 203 to 201 nm (Fig. 2 *B*). This second finding further suggests that NaCl induces a small but noticeable decrease in helicity of pHLIP. Although the differences at 222 nm could conceivably arise from errors in quantification of the peptide, the shift of the minimum is more revealing, increasing our confidence that the presence of NaCl disfavors local helical formation in pHLIP. On the other hand, NaCl did not affect helical formation in state III (pH 3.8), as shown in Fig. S1 (36).

To understand how changes in salt concentration can cause conformational rearrangements in state II, we carried out additional fluorescence experiments with pHLIP conjugated to NBD. As NBD partitions into a more hydrophobic environment, such as the membrane surface, its FI increases (37). Binding of pHLIP-NBD to lipid vesicles increases the fluorescence in a hyperbolic fashion (38) as it transitions from solution (state I) to the lipid vesicle surface (state II) (Fig. S2). We quantified the relative fluorescence increase

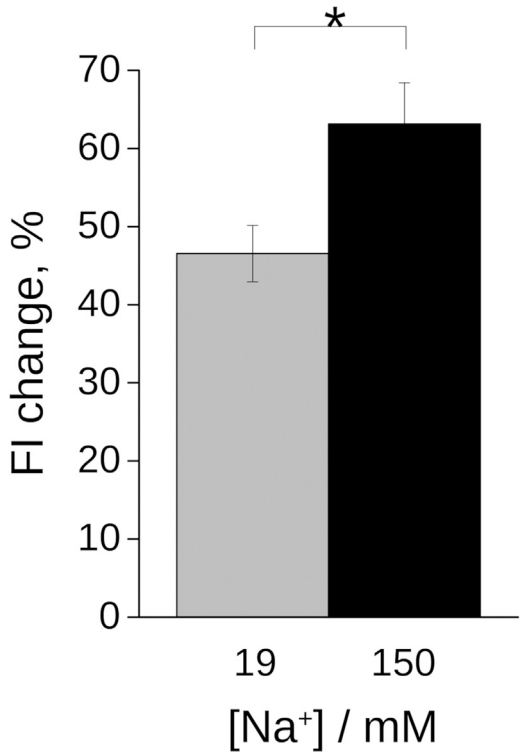

FIGURE 3 Higher levels of Na^+ lead to different FI changes of NBD conjugated to the C_t of pHLIP in state II. Quantification of changes in FI are shown as percentage changes. Experiments were performed in conditions in which similar lipid binding saturation was achieved (0.7 mM POPC, see Fig. S2). Mean and SD are shown. $n = 7$. Statistical analysis was performed with a two-tailed Student's t-test; $^*p < 0.05$.

of NBD in the absence and presence of NaCl. The results in state II showed a larger enhancement of NBD fluorescence in the presence of NaCl (Fig. 3). This data suggests that NaCl induces a change in the environment of the C_t of pHLIP (i.e., where the dye is conjugated). However, the specific molecular events associated to these changes are challenging to elucidate experimentally.

To gain a more complete understanding of the molecular basis of the observed differences, we performed all-atom MD simulations. Our system setup consisted of an unstructured conformation of pHLIP in solution placed above a model POPC bilayer. This was chosen to allow pHLIP to freely bind to and dissociate from the surface of the bilayer. We performed five independent 400-ns simulations at five different NaCl concentrations and observed that the binding of pHLIP was both transient and long lived (>100 ns) (Fig. 4). Multiple association and dissociation events were observed, regardless of the NaCl concentration. When stable binding does occur, it is often associated with an increase in the number of hydrogen bonds between pHLIP and the bilayer surface. Analysis of the average distance between pHLIP and the bilayer surface does not show any discernible changes as a function of salt concentration. Our modeling results suggest that the affinity of pHLIP for the membrane in state II is not affected by an increase in salt concentration. This observation agrees with the experimental determination of the partition coefficient (K_p) of pHLIP to POPC (Fig. S2), which shows that K_p is similar in the absence ($1.5 \pm 0.4 \times 10^5$) or presence of NaCl ($1.7 \pm 0.5 \times 10^5$). Overall, our simulations agree with the experiment; pHLIP remains in close proximity to the surface of the bilayer, as shown by the distance between the COM of pHLIP from the bilayer surface (Fig. S3).

We next examined the interactions Na^+ ions establish with both pHLIP and POPC. We observed that an increase in salt concentration does not affect coordination of Na^+ ions with the PC headgroups, which form the first coordination shell at ~2.2 Å from the oxygen atoms in the phosphate moiety (Fig. S4 *A*). We saw a very slight decrease in the radial distribution function (RDF) at the second coordination shell with an increase in Na^+ concentration. The residence times of Na^+ within 2.5 Å of the phosphate oxygens shows that it is largely unchanged with respect to concentration (1.0–1.1 ns) (Fig. S4 *B*). This is long enough for a Na^+ cation to coordinate with up to four PC headgroups (Fig. S4 *C*). Our residence times are consistent with previous studies on the binding of Na^+ ions to headgroup regions for the CHARMM c36 lipid force field (39), and the coordination of Na^+ ions with PC headgroups is consistent with previous MD studies on PC bilayers (40,41). However, we observed larger changes in the interaction of pHLIP with Na^+. Specifically, we saw a clear broadening of the RDF with increasing salt concentration for Na^+ ions with respect to the C_t acidic residues of pHLIP (Fig. S4 *D*). This broadening becomes noticeable above 20 mM NaCl. The residence time of Na^+ ions with the C-terminal acidic residues is between 300 and 400 ps at all salt concentrations (Fig. S4 *E*). This time frame is long enough to allow for the coordination of cations with the negatively charged acidic residues; for example, at the highest concentration tested (150 mM NaCl), a sodium ion can coordinate between two carboxylate groups on the side chains of D31 and D33, screening the charge-charge repulsion of these two neighboring residues (Fig. S4, *F* and *G*).

Increase in salt concentration has a greater effect on the C_t half of pHLIP

We observed a clear trend in the overall Na^+ RDF of pHLIP—an increase in salt concentration leads to a decrease in specific coordination of Na^+ ions around pHLIP (Fig. 5 *A*). However, salt concentration has no effect on the overall shape of pHLIP as it interacts with the bilayer surface (Fig. S5), which is consistent with our observation that salt concentration has no effect on the binding of pHLIP to the POPC surface. It is only when we look at the interactions of Na^+ ions with specific residues in pHLIP that noticeable differences occur as a function of salt concentration. On the C_t of pHLIP, a significant increase in interaction

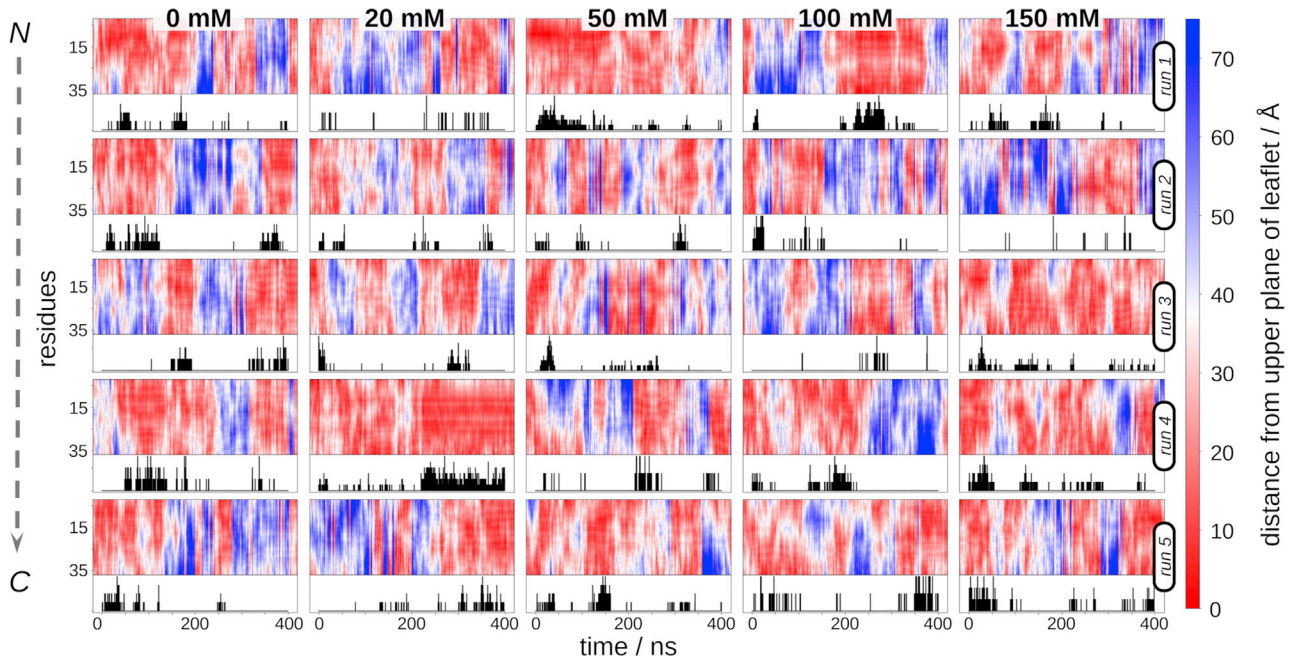

FIGURE 4 Binding of pHLIP to POPC is independent of salt concentration. Shown is the z projection of distance of C_α of every residue in pHLIP from the center of mass (COM) of P atoms of the nearest leaflet in the POPC bilayer. Each row is an independent simulation. Red: bound to the surface; blue: dissociated from POPC. Color-coded distances are represented by the heat bar on the right. Bottom: Dots represent the number of hydrogen bonds between pHLIP and POPC as a function of time. To see this figure in color, go online.

of Na^+ ions with the acidic groups (D31, D33, E34, and the carboxy C_t) takes place, whereas the effect of a higher salt concentration is much less at the protonation switches (D14 and D25) and the N_t acidic residue (E3) (Fig. 5 *B*). In addition, we observed that the coordination of Na^+ ions with the C_t residues generally leads to an increase in the formation of an $i + 3$ salt bridge between R11 and D14 (Fig. 5 *C*). Essentially, as more sodium ions are coordinated with C_t residues of pHLIP, D14 has an increased availability as a complementary partner to the positively charged R11. This type of interaction is a hallmark of peptide folding and a phenomena that transiently occurs in our previous simulations of pHLIP (42,43). When combined with our analysis of the radius of gyration of pHLIP, these data suggest that Na^+ binding to the carboxylates of the C_t acidic residues contributes to the observed p*K* changes.

We also observed changes in the helicity profile of pHLIP as a function of salt concentration (Fig. 2). At a low salt concentration, the N-terminal half of pHLIP shows a greater tendency to form an α-helix (Fig. 6 *A*). As the concentration of NaCl increases, the C-terminal acidic residues are screened by Na^+ ions, leading to a significant increase in helicity around the sinker stretch (L21 to V30). However, an increase in salt concentration does not induce a noticeable effect on the overall helicity of pHLIP; regardless of concentration, pHLIP still forms only one helical turn (i.e., five residues) (Fig. 6 *B*). In combination with our experimental results, we can now show that salt

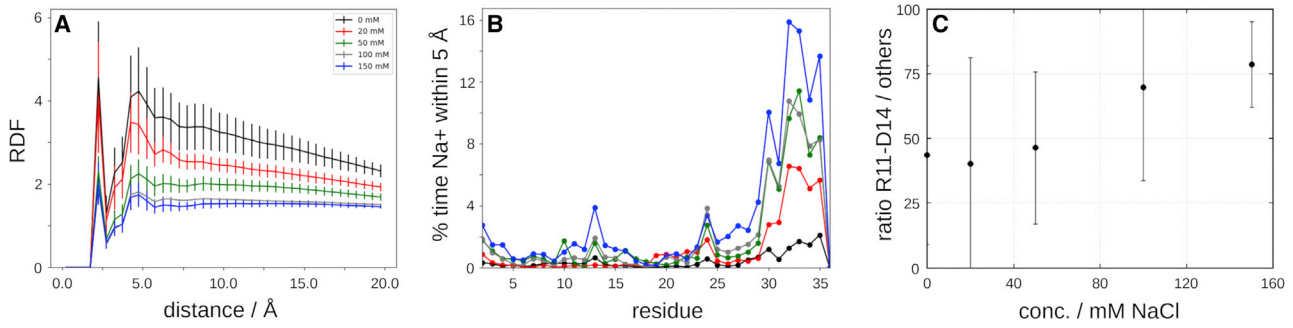

FIGURE 5 Increasing salt concentration affects intramolecular interactions in pHLIP. (*A*) Radial distribution function (RDF) of Na^+ ions around pHLIP (0 mM contains five neutralizing ions). (*B*) Percentage of time when a Na^+ ion is within 5 Å of each residue. (*C*) Percentage of time R11 forms a salt bridge with each of the acidic residues in pHLIP. The color scheme in the legend applies to (*A–C*). To see this figure in color, go online.

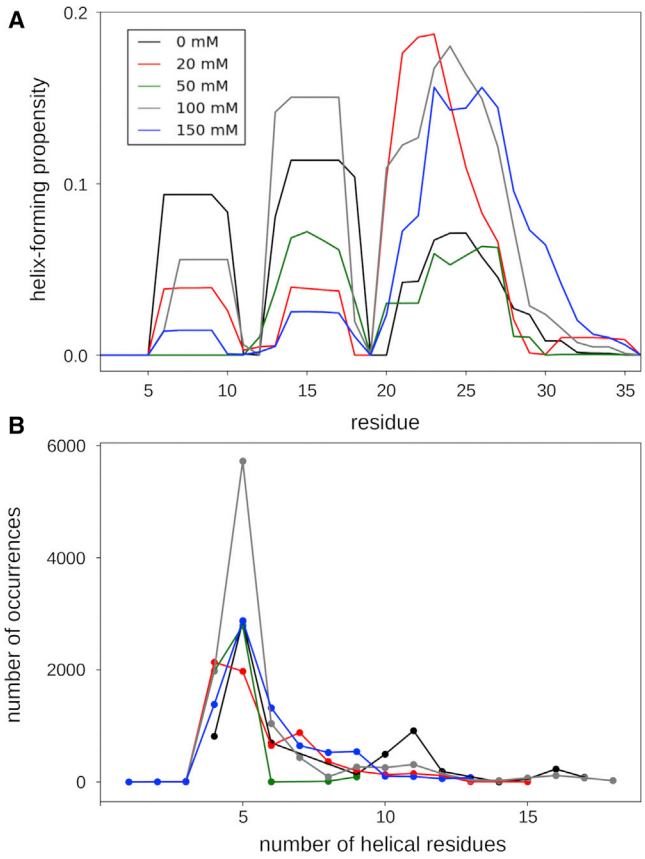

FIGURE 6 Increase in salt concentration modulates localized formation of helices in state II. (*A*) Per-residue helix-forming propensity of pHLIP as a function of salt concentration is shown. (*B*) Overall helix-forming propensity of pHLIP as a function of salt concentration. To see this figure in color, go online.

concentration has definitive localized effects on the conformational sampling of pHLIP, whereas in state II, pHLIP still generally remains in a random coil conformation.

DISCUSSION

When unstructured peptides or small proteins, such as α-synuclein, partition to the surface of lipid membranes, they typically gain helical structure (44,45). Secondary structure formation is favored because of the increased propensity to form hydrogen bonds in the backbone chain. However, pHLIP and other pH-responsive membrane peptides such as ATRAM (38) and TYPE7 (46) bind to membranes in a disordered state. How such peptides remain stable on the lipid surface in unstructured conformations is poorly understood.

We evaluated the membrane interaction of pHLIP using a concentration of NaCl similar to that found in blood serum. Our fluorescence data show that an increase in salt concentration to physiological levels strongly drives down the pK of insertion of pHLIP (Fig. 1). With the aid of our MD simulations, we can hypothesize that this change in the pK of insertion is due to a combination of the effect of an increased number of salt ions on pHLIP and the bilayer. In the case of pHLIP, the higher salt concentration induces an electrostatic competition between the excess sodium ions and protons in solution for the titratable side chains of the peptide. Previous spectroscopic and computational studies have shown that sodium binds preferentially to the carboxylate side chains of acidic residues in proteins and small peptides (42,47–50). In addition, sodium ions show a higher propensity to bind to aspartic acid residues over glutamic acid residues (51). In general, we observe a higher rate of interaction of sodiums with the aspartic acids in pHLIP (D14, D25, D31, and D33) over the glutamic acids (E3 and E34); the higher rate of interaction of E34 is most likely environment-dependent because it is proximal to D31, D33, and the negatively charged C_t. The overall result of this increased interaction of acidic residues with sodium is that the titratable sites of pHLIP are being competitively inhibited. Shifting from a p$K_{\text{Ct-NBD}}$ of 5.2 at 19 mM Na^+ to 4.6 at 150 mM Na^+ is equivalent to a fourfold increase in proton concentration (6.3–25.1 μM) that is required to achieve state III. Therefore, this is not a completely direct competition as it requires a 7.9-fold increase in sodium ions (19–150 mM) compared to the fourfold increase in protons. This excess of sodium ions indicates that other components of our system (i.e., the lipid bilayer) may also be affected by higher salt concentrations.

As salt concentration increases, sodium cations have a higher likelihood of coordinating multiple PC headgroups, leading to a decrease in area per lipid and an increase in bilayer thickness (Figs. S6 and S7; (40,41)). In our case, this "stiffening" of the bilayer could prevent pHLIP from partitioning more deeply into the headgroup region, similar to what Larson and co-workers observed in MD simulations of magainin binding to a POPC bilayer (52). However, an increase in salt concentration was also shown to create a positive electrostatic potential at the surface of the bilayer (40), which would lead to a more productive binding surface for the negatively charged pHLIP in state II. The two opposing phenomena help explain the subtle balance that is affected by the presence of salt; we do not see an overall decrease in the quality of binding (K_p) of pHLIP to POPC at higher salt concentrations because of the potential electrostatic attraction between the peptide and the lipids, but we also do not observe deeper partitioning of pHLIP due to the more rigid behavior of the bilayer. It has been previously reported that the concentration of sodium phosphate affected the pK of pHLIP (10). Specifically, the pK was slightly higher in the presence of 20 mM than in 55 mM sodium phosphate, opposite to what we observed (Fig. 1 *B*). However, under those conditions, the aggregation of pHLIP occurred, suggesting that aggregation effects were responsible for the observed results.

Our state II CD data show that the presence of NaCl induces a statistically significant local decrease in the helicity

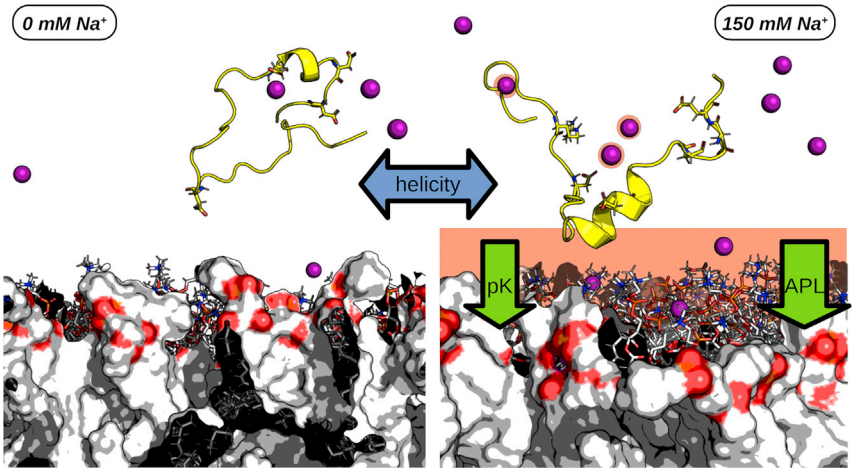

FIGURE 7 How increased salt concentration alters the acid sensitivity of pHLIP. Schematic of pHLIP in the absence and presence of salt. Left: In the absence of salt, pHLIP freely interacts with the bilayer surface. Right: However, as the concentration of salt increases (highlighted in *salmon*), it competitively inhibits protonation of the acidic residues in pHLIP, altering its behavior in several ways: 1) a shift in localized helicity in state II, 2) a decrease in the area per lipid of the bilayer (i.e., stiffening), and 3) a decrease in the p*K* of pHLIP. Spheres: sodium ions; ribbons: pHLIP; yellow sticks: acidic residues in pHLIP; white sticks: POPC lipids; and surface: POPC lipids. To see this figure in color, go online.

of pHLIP. However, it is important to clarify that in the experimental conditions used to study state II, there are actually a mix of two conformations, pHLIP in state I and state II. Through our K_p measurements in these conditions, we calculate that only ~50% of pHLIP is bound to the membrane, and thus, the full extent of the effect of NaCl on helix formation is most likely underestimated. There is precedent for our observation of a correlation between helicity and salt concentration. Previous MD simulations showed that the binding of sodium ions to carboxylate side chains of acidic residues screen electrostatic repulsion with other negatively charged residues (49,50). When residues are proximal to one another, like for D25, D31, D33, and E34 in pHLIP, this screening allows for closer intramolecular interactions (51) and potentially lowers the barrier for folding into an α-helix. This folding phenomenon associated with higher salt concentrations has also been observed in the villin headpiece, where binding of chloride anions bound to positively charged residues lowered the energy barrier to fold into a native-like conformation (53). Some of the earliest work on protein folding demonstrated that ionic strength as weak as 150 mM was sufficient to induce helical formation in neutral peptides (54), explicitly identifying the connection between salt concentration and secondary structure. The aforementioned studies were conducted on soluble proteins; in the case of pHLIP, we must account for interactions with the bilayer. Cell-penetrating peptides experience "partitioning-folding coupling," a phenomena in which short peptides will fold into an α-helix after partitioning into the headgroup region because of the fact that it is more energetically favorable to partition a hydrogen-bonded, helical backbone into the bilayer than a coiled polypeptide (55,56). Without the aid of titration of the acidic residues in pHLIP at lower pH levels, pHLIP will undergo minimal folding into a helix when bound to the bilayer surface. At higher salt concentrations, this propensity to form a helix can shift because of electrostatic screening of the carboxylate side chains by sodium cations as shown in our MD simulations. In addition, the increasing stiffness of the bilayer at higher salt concentrations can potentially prevent pHLIP from partitioning into a more energetically favorable hydrophobic region (Fig. 7). In combination with our CD experiments that show a small but significant decrease in helicity, this provides a detailed picture of how higher salt concentrations can lead to a decrease in the p*K* of insertion of pHLIP.

The altered interactions of pHLIP with the POPC surface we observed agree well with recent work (18,19). Upon introducing different lipids to create heterogeneous membrane environments, intrinsic fluorescence spectroscopy reveals that state II becomes spectroscopically silent; even though pHLIP would bind to the lipid vesicle surface, binding is so shallow that the environment surrounding W9 and W15 in pHLIP remains unchanged from state I. In addition, any other lipid composition besides 100% POPC would typically lead to a slight decrease in the p*K* of insertion (5.7–6.2). This shallow conformation was named "state II^{S}" and was accompanied by a decrease in the p*K* of insertion. In a similar manner, by increasing the salt concentration, we are also altering interfacial interactions between pHLIP and the bilayer, so it is not surprising that we observe a decrease in the p*K* of insertion as well.

CONCLUSIONS

This work advances the understanding of the role of electrostatics in the interactions between pHLIP and membranes. We show that small electrostatic changes on state II have a powerful effect on the acidity required for membrane insertion. The effectiveness of pHLIP for the targeted delivery of drugs to tumors is incumbent on the agreement between the extracellular pH found in the tumor environment and the p*K* of pHLIP. Our results indicate that modulating the electrostatic interactions in state II, which could be achieved by conservative changes in the sequence of pHLIP, may be an effective means to control

the pK of pHLIP. Ultimately, our biophysical study underscores how pHLIP is influenced by a multitude of factors that must be accounted for to advance our fundamental understanding of its function.

SUPPORTING MATERIAL

Supporting Material can be found online at https://doi.org/10.1016/j.bpj.2019.07.034.

AUTHOR CONTRIBUTIONS

B.M. and F.N.B. designed the research. J.W., C.G., H.L.S., Y.Y., and A.C. carried out all the experiments and simulations. J.W., C.G., H.L.S., Y.Y., A.C., B.M., and F.N.B. analyzed the data and wrote the article.

ACKNOWLEDGMENTS

We are thankful to members of the Barrera and Mertz laboratories for scientific discussions and comments on the manuscript.

This work was partially supported by National Institute of Health grants R01GM120642 (to F.N.B.) and R15GM120676 (to B.M.).

REFERENCES

1. Hunt, J. F., P. Rath, …, D. M. Engelman. 1997. Spontaneous, pH-dependent membrane insertion of a transbilayer α-helix. *Biochemistry.* 36:15177–15192.
2. Reshetnyak, Y. K., M. Segala, …, D. M. Engelman. 2007. A monomeric membrane peptide that lives in three worlds: in solution, attached to, and inserted across lipid bilayers. *Biophys. J.* 93:2363–2372.
3. Hanz, S. Z., N. S. Shu, …, W. Qiang. 2016. Protonation-driven membrane insertion of a pH-low insertion peptide. *Angew. Chem. Int.Engl.* 55:12376–12381.
4. Otieno, S. A., S. Z. Hanz, …, W. Qiang. 2018. pH-dependent thermodynamic intermediates of pHLIP membrane insertion determined by solid-state NMR spectroscopy. *Proc. Natl. Acad. Sci. USA.* 115:12194–12199.
5. Deacon, J. C., D. M. Engelman, and F. N. Barrera. 2015. Targeting acidity in diseased tissues: mechanism and applications of the membrane-inserting peptide, pHLIP. *Arch. Biochem. Biophys.* 565:40–48.
6. Andreev, O. A., A. G. Karabadzhak, …, Y. K. Reshetnyak. 2010. pH (low) insertion peptide (pHLIP) inserts across a lipid bilayer as a helix and exits by a different path. *Proc. Natl. Acad. Sci. USA.* 107:4081–4086.
7. Musial-Siwek, M., A. Karabadzhak, …, D. M. Engelman. 2010. Tuning the insertion properties of pHLIP. *Biochim. Biophys. Acta.* 1798:1041–1046.
8. Barrera, F. N., D. Weerakkody, …, D. M. Engelman. 2011. Roles of carboxyl groups in the transmembrane insertion of peptides. *J. Mol. Biol.* 413:359–371.
9. Karabadzhak, A. G., D. Weerakkody, …, Y. K. Reshetnyak. 2012. Modulation of the pHLIP transmembrane helix insertion pathway. *Biophys. J.* 102:1846–1855.
10. Fendos, J., F. N. Barrera, and D. M. Engelman. 2013. Aspartate embedding depth affects pHLIP's insertion pKa. *Biochemistry.* 52:4595–4604.
11. Weerakkody, D., A. Moshnikova, …, Y. K. Reshetnyak. 2013. Family of pH (low) insertion peptides for tumor targeting. *Proc. Natl. Acad. Sci. USA.* 110:5834–5839.
12. Onyango, J. O., M. S. Chung, …, M. An. 2015. Noncanonical amino acids to improve the pH response of pHLIP insertion at tumor acidity. *Angew. Chem. Int.Engl.* 54:3658–3663.
13. Shu, N. S., M. S. Chung, …, W. Qiang. 2015. Residue-specific structures and membrane locations of pH-low insertion peptide by solid-state nuclear magnetic resonance. *Nat. Commun.* 6:7787.
14. Tapmeier, T. T., A. Moshnikova, …, R. J. Muschel. 2015. The pH low insertion peptide pHLIP Variant 3 as a novel marker of acidic malignant lesions. *Proc. Natl. Acad. Sci. USA.* 112:9710–9715.
15. Wyatt, L. C., A. Moshnikova, …, Y. K. Reshetnyak. 2018. Peptides of pHLIP family for targeted intracellular and extracellular delivery of cargo molecules to tumors. *Proc. Natl. Acad. Sci. USA.* 115:E2811–E2818.
16. Barrera, F. N., J. Fendos, and D. M. Engelman. 2012. Membrane physical properties influence transmembrane helix formation. *Proc. Natl. Acad. Sci. USA.* 109:14422–14427.
17. Scott, H. L., V. P. Nguyen, …, F. N. Barrera. 2015. The negative charge of the membrane has opposite effects on the membrane entry and exit of pH-low insertion peptide. *Biochemistry.* 54:1709–1712.
18. Kyrychenko, A., V. Vasquez-Montes, …, A. S. Ladokhin. 2015. Lipid headgroups modulate membrane insertion of pHLIP peptide. *Biophys. J.* 108:791–794.
19. Vasquez-Montes, V., J. Gerhart, …, A. S. Ladokhin. 2018. Comparison of lipid-dependent bilayer insertion of pHLIP and its P20G variant. *Biochim. Biophys. Acta. Biomembr.* 1860:534–543.
20. Connor, J., C. Bucana, …, A. J. Schroit. 1989. Differentiation-dependent expression of phosphatidylserine in mammalian plasma membranes: quantitative assessment of outer-leaflet lipid by prothrombinase complex formation. *Proc. Natl. Acad. Sci. USA.* 86:3184–3188.
21. Ladokhin, A. S., S. Jayasinghe, and S. H. White. 2000. How to measure and analyze tryptophan fluorescence in membranes properly, and why bother? *Anal. Biochem.* 285:235–245.
22. Scott, H. L., J. M. Westerfield, and F. N. Barrera. 2017. Determination of the membrane translocation pK of the pH-low insertion peptide. *Biophys. J.* 113:869–879.
23. Gupta, C., and B. Mertz. 2017. Protonation enhances the inherent helix-forming propensity of pHLIP. *ACS Omega.* 2:8536–8542.
24. Jo, S., T. Kim, …, W. Im. 2008. CHARMM-GUI: a web-based graphical user interface for CHARMM. *J. Comput. Chem.* 29:1859–1865.
25. Brooks, B. R., C. L. Brooks, III, …, M. Karplus. 2009. CHARMM: the biomolecular simulation program. *J. Comput. Chem.* 30:1545–1614.
26. Lee, J., X. Cheng, …, W. Im. 2016. CHARMM-GUI input generator for NAMD, GROMACS, AMBER, OpenMM, and CHARMM/OpenMM simulations using the CHARMM36 additive force field. *J. Chem. Theory Comput.* 12:405–413.
27. Wu, E. L., X. Cheng, …, W. Im. 2014. CHARMM-GUI Membrane Builder toward realistic biological membrane simulations. *J. Comput. Chem.* 35:1997–2004.
28. Phillips, J. C., R. Braun, …, K. Schulten. 2005. Scalable molecular dynamics with NAMD. *J. Comput. Chem.* 26:1781–1802.
29. Maier, J. A., C. Martinez, …, C. Simmerling. 2015. ff14SB: improving the accuracy of protein side chain and backbone parameters from ff99SB. *J. Chem. Theory Comput.* 11:3696–3713.
30. Dickson, C. J., B. D. Madej, …, R. C. Walker. 2014. Lipid14: the amber lipid force field. *J. Chem. Theory Comput.* 10:865–879.
31. Izadi, S., R. Anandakrishnan, and A. V. Onufriev. 2014. Building water models: a different approach. *J. Phys. Chem. Lett.* 5:3863–3871.
32. Case, D. A., R. M. Betz, …, P. Kollman. 2016. Amber16. University of California, San Francisco.
33. Humphrey, W., A. Dalke, and K. Schulten. 1996. VMD: visual molecular dynamics. *J. Mol. Graph.* 14:33–38., 27–28.
34. Frishman, D., and P. Argos. 1995. Knowledge-based protein secondary structure assignment. *Proteins.* 23:566–579.
35. Kelly, S. M., T. J. Jess, and N. C. Price. 2005. How to study proteins by circular dichroism. *Biochim. Biophys. Acta.* 1751:119–139.

36. Kelly, S. M., and N. C. Price. 2000. The use of circular dichroism in the investigation of protein structure and function. *Curr. Protein Pept. Sci.* 1:349–384.

37. Chattopadhyay, A. 1990. Chemistry and biology of N-(7-nitrobenz-2-oxa-1,3-diazol-4-yl)-labeled lipids: fluorescent probes of biological and model membranes. *Chem. Phys. Lipids.* 53:1–15.

38. Nguyen, V. P., D. S. Alves, …, F. N. Barrera. 2015. A novel soluble peptide with pH-responsive membrane insertion. *Biochemistry.* 54:6567–6575.

39. Venable, R. M., Y. Luo, …, R. W. Pastor. 2013. Simulations of anionic lipid membranes: development of interaction-specific ion parameters and validation using NMR data. *J. Phys. Chem. B.* 117:10183–10192.

40. Pandit, S. A., D. Bostick, and M. L. Berkowitz. 2003. Molecular dynamics simulation of a dipalmitoylphosphatidylcholine bilayer with NaCl. *Biophys. J.* 84:3743–3750.

41. Böckmann, R. A., A. Hac, …, H. Grubmüller. 2003. Effect of sodium chloride on a lipid bilayer. *Biophys. J.* 85:1647–1655.

42. Marqusee, S., and R. L. Baldwin. 1987. Helix stabilization by Glu-...Lys+ salt bridges in short peptides of de novo design. *Proc. Natl. Acad. Sci. USA.* 84:8898–8902.

43. Gupta, C., Y. Ren, and B. Mertz. 2018. Cooperative nonbonded forces control membrane binding of the pH-low insertion peptide pHLIP. *Biophys. J.* 115:2403–2412.

44. White, S. H., W. C. Wimley, …, K. Hristova. 1998. [4] Protein folding in membranes: determining energetics of peptide-bilayer interactions. *In* Methods in Enzymology, Energetics of Biological Macromolecules Part B, *Volume 295*. G. K. Ackers and M. L. Johnson, eds.. Academic Press, pp. 62–87.

45. Dikiy, I., and D. Eliezer. 2012. Folding and misfolding of alpha-synuclein on membranes. *Biochim. Biophys. Acta.* 1818:1013–1018.

46. Alves, D. S., J. M. Westerfield, …, F. N. Barrera. 2018. A novel pH-dependent membrane peptide that binds to EphA2 and inhibits cell migration. *eLife.* 7:e36645.

47. Vrbka, L., J. Vondrásek, …, P. Jungwirth. 2006. Quantification and rationalization of the higher affinity of sodium over potassium to protein surfaces. *Proc. Natl. Acad. Sci. USA.* 103:15440–15444.

48. Uejio, J. S., C. P. Schwartz, …, R. J. Saykally. 2008. Characterization of selective binding of alkali cations with carboxylate by x-ray absorption spectroscopy of liquid microjets. *Proc. Natl. Acad. Sci. USA.* 105:6809–6812.

49. Dzubiella, J. 2009. Salt-specific stability of short and charged alanine-based α-helices. *J. Phys. Chem. B.* 113:16689–16694.

50. Dzubiella, J. 2010. Molecular insights into the ion-specific kinetics of anionic peptides. *J. Phys. Chem. B.* 114:7098–7103.

51. Friedman, R. 2011. Ions and the protein surface revisited: extensive molecular dynamics simulations and analysis of protein structures in alkali-chloride solutions. *J. Phys. Chem. B.* 115:9213–9223.

52. Kandasamy, S. K., and R. G. Larson. 2006. Effect of salt on the interactions of antimicrobial peptides with zwitterionic lipid bilayers. *Biochim. Biophys. Acta.* 1758:1274–1284.

53. Yoda, T., Y. Sugita, and Y. Okamoto. 2014. Salt effects on hydrophobic-core formation in folding of a helical miniprotein studied by molecular dynamics simulations. *Proteins.* 82:933–943.

54. Scholtz, J. M., E. J. York, …, R. L. Baldwin. 1991. A neutral, water-soluble, .alpha.-helical peptide: the effect of ionic strength on the helix-coil equilibrium. *J. Am. Chem. Soc.* 113:5102–5104.

55. Ladokhin, A. S., and S. H. White. 1999. Folding of amphipathic alpha-helices on membranes: energetics of helix formation by melittin. *J. Mol. Biol.* 285:1363–1369.

56. Almeida, P. F., A. S. Ladokhin, and S. H. White. 2012. Hydrogen-bond energetics drive helix formation in membrane interfaces. *Biochim. Biophys. Acta.* 1818:178–182.